

Project and Probe: Sample-Efficient Domain Adaptation by Interpolating Orthogonal Features

Annie S. Chen^{*1}, Yoonho Lee^{*1}, Amrith Setlur², Sergey Levine³, Chelsea Finn¹

Stanford University¹, Carnegie Mellon University², UC Berkeley³

asc8@stanford.edu, yoonho@stanford.edu

Abstract

Transfer learning with a small amount of target data is an effective and common approach to adapting a pre-trained model to distribution shifts. In some situations, target data labels may be expensive to obtain, so we may only have access to a limited number of target data points. To make the most of a very small target dataset, we propose a lightweight, sample-efficient approach that learns a diverse set of features and adapts to a target distribution by interpolating these features. Our approach, PROJECT AND PROBE (PRO²), first learns a linear projection that maps a pre-trained embedding onto orthogonal directions while being predictive of labels in the source dataset. The goal of this step is to learn a variety of predictive features, so that at least some of them remain useful after distribution shift. PRO² then learns a linear classifier on top of these projected features using a small target dataset. Theoretically, we find that PRO² results in more sample-efficient generalization by inducing a favorable bias-variance tradeoff. Our experiments on four datasets, with multiple distribution shift settings for each, show that PRO² improves performance by 5-15% when given limited target data compared to prior methods such as standard linear probing.

1 Introduction

Machine learning models can face significant challenges when there is a distribution shift between training and evaluation data. A model trained on a specific source dataset may not perform well when deployed on a target domain with a distribution of inputs that differs significantly from the source domain. One common and reliable approach for adapting to distribution shifts is fine-tuning a trained model on a small amount of labeled data from the new target domain. However, in some situations, target data labels may be expensive to obtain, which limits the number of available labeled datapoints for fine-tuning. As an example, a hospital may have imaging software that slightly differs from what was used for dataset collection, but they may not be able to acquire many new labeled samples. In such conditions, conventional fine-tuning approaches may overfit to the small target dataset and distort the information learned during initial training. Therefore, we require a method that can reliably extract information from the new target domain with less overfitting.

Recent works have demonstrated the effectiveness of re-training a final linear head using target data for adapting to distribution shifts due to spurious correlations or domain shift [43, 21, 36]. However, it is unclear whether this standard approach of re-training a linear layer is the most data-efficient method to adapt pre-trained features to various target distributions. While versatile, feature embeddings may not necessarily contain the most suitable set of features for adapting to target distributions: they may also contain redundant, non-predictive, or noisy information. Our primary insight is that the key to more sample-efficient adaptation to target domains lies in starting with a compact and diverse set of useful features. Each feature in this set should not only be predictive, but also hold unique information distinct from others inside the set. We leverage source data, which

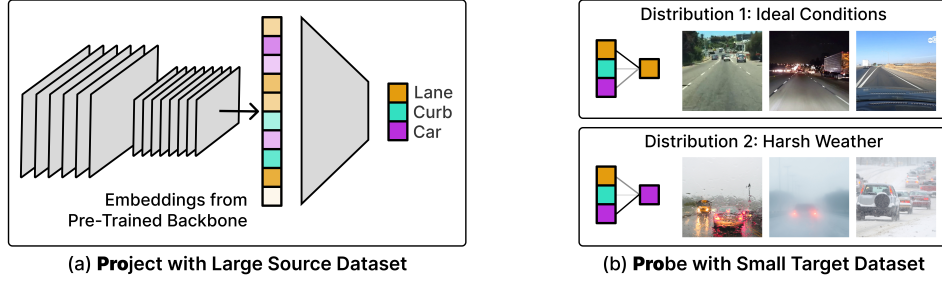


Figure 1: **The Project and Probe (PRO²) framework for adapting to different target distributions.** (a) We first use a large source dataset to project pre-trained feature embeddings onto a set of predictive features while enforcing orthogonality. (b) For a new target distribution, we learn a linear layer on top of the projected features. This step adaptively chooses features in a data-efficient manner.

is substantially more abundant than target data, in performing this selection of features for target adaptation.

We propose PROJECT AND PROBE (PRO²), a simple and sample-efficient method for adapting to unknown target distributions. PRO² first learns a projection of pre-trained embedding vectors, which is optimized to extract a diverse set of features that are each predictive of labels. More specifically, we first use a source dataset to project pre-trained feature embeddings onto a smaller set of predictive features. We enforce pairwise orthogonality among all features, thereby ensuring that each projected dimension carries unique information not present in others. We expect this learned feature space to compactly contain a diverse set of predictive features while discarding information that is redundant or not predictive on the task. PRO² then uses the reduced set of features as a basis space for adaptation. Specifically, we fit a linear head on top of the projected embedding using labeled target data. Both the linear projection and the linear head require minimal computational overhead, making PRO² a practical method for adapting to new target distributions. Fig. 1 shows a visual summary of PRO².

To support our approach, we provide a theoretical analysis, in both a general setting with minimal distribution assumptions as well as the more specific setting of a shifted homoscedastic Gaussian model, showing how PRO² learns a projection matrix that results in better generalization due to a favorable bias-variance tradeoff. From this analysis, PRO² improves sample efficiency because it can learn useful, diverse features so that it is more likely to better recover the important directions for adaptation with a smaller projection dimension, allowing us to combat the variance introduced by a very small target dataset while maintaining low bias. We conduct experiments on a variety of distribution shift settings across 4 datasets. We find that standard linear probing, which is the default method used by prior works, is not the most data-efficient adaptation approach. Using PRO², i.e. projecting with source data onto an informative feature-space basis and probing with target data, improves performance by 5-15% in few-shot adaptation to new target distributions.

2 Related Work

Robustness and zero-shot generalization. Many prior works aim to improve robustness to various distribution shifts [54, 14, 2, 44, 38, 8, 30, 63]. Additionally, prior works have studied how to adapt pre-trained features to a target distribution via fine-tuning [39, 60, 48]. Such fine-tuning works typically frame robustness to distribution shift as a zero-shot generalization problem [23, 61, 58, 24], where the model is trained on source and evaluated on target. Both of the above classes of approaches fundamentally cannot handle the problem settings we consider, where a single function is insufficient for achieving good performance on different distributions. In this paper, we evaluate on a variety of test distributions, some of which are mutually exclusive, and it is therefore crucial to perform adaptation on the target distribution.

Adapting to distribution shifts. Recent works have proposed various methods for adapting models at test time with some labeled target data [50, 55, 18, 57, 62, 13, 26]. In particular, given a feature embedding produced by a pretrained network with sufficient expressivity, training a final linear head, also known as linear probing, suffices for adapting to datasets with spurious correlations [21, 36, 19]

as well as in the setting of domain generalization [43]. As detailed further in Sec. 3, we specifically focus on scenarios in which we have very little target data (only $4 \sim 256$ datapoints). We find that in this setting, training a final linear head in the default manner is not the most data-efficient way to adapt. PRO², which breaks this training down into 2 steps, is able to more effectively extract useful features and interpolate between them for varying target distributions, leading to improved sample efficiency with limited target data.

Learning diverse features for spurious datasets. Neural networks tend to be biased towards learning simple functions that rely on shortcut features [3, 16, 47, 15, 42, 29, 34]. To better handle novel distributions, it is important to consider the entire set of functions that are predictive on the training data [12, 46, 59]. Recent diversification methods discover such a set [52, 40, 27]. The latter two methods use additional assumptions such as unlabeled data. With a similar motivation to ours, Teney et al. [52] penalizes the similarity between different features, but does so with an additional loss term instead of explicitly enforcing orthogonality. We observe that this implementation detail matters in Sec. 6, where PRO² outperforms Teney et al. [52]. A concurrent work [37] also proposes an orthogonal projection method to learn diverse classifiers. However, the Probe step of PRO² additionally interpolates between the orthogonal features, and we provide theoretical and empirical analysis of how distribution shift severity affects sample efficiency during probing.

Compression & feature selection. In aiming to extract important features and discarding repetitive information, PRO² is related to work on compression [35] and information bottlenecks [53, 1]. Our method is also closely related to methods that learn projections such as principal component analysis (PCA) and linear discriminant analysis (LDA). Beyond these representative methods, there is an immense body of work on feature selection [10, 31, 7, 28] and dimensionality reduction [25, 49, 9]. Among all projection-based methods, LDA is the most related to ours, but it only learns the single most discriminative direction. In Corollary 9, we show that PRO² with dimensionality $d = 1$ provably recovers the LDA direction in a shifted homoscedastic Gaussian model, and that using higher values of d is critical in adapting to higher degrees of distribution shift. Generally, most methods (including LDA) operate in the setting without distribution shift.

3 Adaptation to Distribution Shift

We now describe our problem setting, where the goal is to adapt a model so as to provide an accurate decision boundary under distribution shift given a limited amount of target distribution information. We consider a source distribution $p_S(x, y)$ and multiple target distributions $p_T^1(x, y), p_T^2(x, y), \dots$. The source dataset $\mathcal{D}_S \in (\mathcal{X} \times \mathcal{Y})^N$ is sampled from the source distribution p_S . We evaluate adaptation to each target distribution p_T^i given a small set of labeled target data $\mathcal{D}_T^i \in (\mathcal{X} \times \mathcal{Y})^M$, where $M \ll N$ so the model must learn from both the source and target data for best performance. We measure the post-adaptation average accuracy of the model on a held-out target dataset from the same distribution p_T^i .

We note that this setting differs from the setting studied in prior works on spurious correlations [44], which train a model only on source data \mathcal{D}_S and evaluate the model’s performance on the hardest target distribution (i.e., worst-group accuracy). This is also different from the setting used in fine-tuning methods for zero-shot generalization [58, 24]: such methods fine-tune a pretrained model on source data \mathcal{D}_S and directly evaluate performance on target data \mathcal{D}_T^i without any exposure to labeled target data. Compared to these zero-shot evaluation settings, we argue that a small amount of target data may realistically be required to handle the arbitrary distribution shifts that arise in the real world. Target data can be an effective point of leverage because it can be available or easy to collect, and we find that even a small dataset can reveal a lot about what features are effective in the target distribution. Our problem setting of adapting with target data has been used in some recent works [21, 43, 19, 26], but we specifically focus on the setting in which we only have access to a very small target dataset, i.e., $M \ll N$.

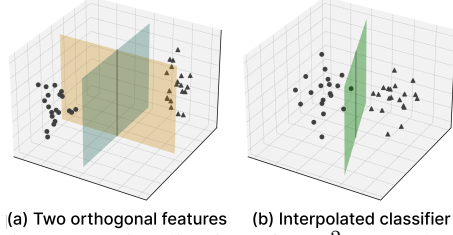
4 Project and Probe

We now describe PRO², a framework for few-shot adaptation to distribution shifts. PRO² is composed of two steps: (1) learn a projection Π that maps pre-trained embeddings onto orthogonal directions, and (2) learn a classifier g using projected embeddings.

Before Step (1), we use a pre-trained backbone model $f : \mathcal{X} \rightarrow \mathbb{R}^D$ to map the datapoints to D -dimensional embeddings. This backbone model extracts meaningful features from the raw inputs,

Algorithm 1 Project and Probe

Input: Source data \mathcal{D}_S , Target data \mathcal{D}_T ,
Backbone $f : \mathcal{X} \rightarrow \mathbb{R}^D$
Initialize $\Pi : \mathbb{R}^D \rightarrow \mathbb{R}^d$ **#Project** with source
for i in $1 \dots d$ **do**
 $\Pi_i \leftarrow \arg \min \mathcal{L}_S(\Pi_i(f(x)), y)$
 subject to $\Pi_j \perp \Pi_i$ for all $j < i$
end for
Initialize $g : \mathbb{R}^d \rightarrow \mathcal{Y}$ **#Probe** with target
 $g \leftarrow \arg \min \mathcal{L}_T(g(\Pi(f(x))), y)$



(a) Two orthogonal features (b) Interpolated classifier
Figure 2: Visualization of PRO²: (a) orthogonal decision boundaries learned during the Project stage, and (b) the interpolated classifier learned during the Probe stage.

resulting in a low-dimensional embedding space, for example $224 \times 224 \times 3$ images to $D = 1024$ -dimensional embeddings.

Step 1: Project with source. Recall that we operate in the few-shot setting, where we may have fewer target datapoints than even embedding dimensions ($M < D$). Intuitively, we would like to select a suitable decision boundary from a set of decision boundaries that worked well in the source domain. If this set is discrete, that might correspond to training some sort of diversified ensemble of linear classifiers on top of the features, a strategy adopted in some prior works [51, 27, 40].

However, in general, we might need the expressive power of a continuous set of decision boundaries to adapt to the target domain, and we can construct this set by *interpolating* over a basis of decision boundaries. Mathematically, this is identical to selecting a set of linear features. Thus, the question we must answer is: which set of linear features of the D -dimensional feature space should we retain? First, it should be clear that the features should form an orthogonal basis, as otherwise they will be redundant. Second, the features should be discriminative, in the sense that they are sufficient to solve the desired prediction task. Lastly, there should not be too many of them, since the more features we include (i.e., the larger the rank of the basis we learn), the more samples we’ll need from the target domain to find the best decision boundary in the corresponding set.

To learn a feature space that satisfies these desiderata, we parameterize a linear projection $\Pi : \mathbb{R}^D \rightarrow \mathbb{R}^d$ that maps the embeddings to a reduced space ($d \leq D$). Specifically, we use the source data to learn a complete orthonormal basis for the embedding space $\Pi_1, \Pi_2, \dots, \Pi_d \in \mathbb{R}^D$, by learning each basis vector with the constraint that it is orthogonal to all vectors before it:

$$\Pi_i = \arg \min_{\Pi_i} \mathbb{E}_{(x,y) \sim \mathcal{D}_S} \mathcal{L}(\Pi_i(f(x)), y) \quad \text{s.t.} \quad \Pi_j \perp \Pi_i \text{ for all } j < i. \quad (\text{PRO}^2)$$

Note that this induces a natural ranking among the basis vectors. This collection of orthogonal vectors constitute the rows of our projection matrix Π . In our implementation, we do projected gradient descent, enforcing orthogonality using QR decomposition on the projection matrix after every gradient step. See Appendix B for a short PyTorch implementation.

Empirically and theoretically, we find that it is particularly beneficial to use a small $d \ll D$, even $d = 1$, in when adapting to small distribution shifts and use larger d for more severe distribution shifts.

Step 2: Probe with target. After learning Π , we learn a classifier $g : \mathbb{R}^d \rightarrow \mathcal{Y}$ that maps the projected embeddings to the target labels:

$$g = \arg \min_{g} \mathbb{E}_{(x,y) \sim \mathcal{D}_T} \mathcal{L}(g(\Pi(f(x))), y).$$

Since the projection Π was optimized to a diverse set of the most discriminative features for the source data, we expect the initial projected features to be particularly predictive when the distribution shift is relatively small.

In summary, PRO² is a simple and lightweight framework that addresses the problem of few-shot adaptation in the presence of distribution shifts. We summarize its overall structure in Algorithm 1 and show a simplified 3D visualization in Fig. 2. In our implementation, we use cached embeddings for all source and target datapoints, such that feeding raw inputs through f is a one-time cost that is amortized over epochs and experiments, making our framework scalable and efficient. As an

orthogonal improvement to our work, one could additionally fine-tune the backbone network on source data. In Sec. 5, we theoretically analyze the properties of the projection and classifier learned by PRO². We then empirically evaluate PRO² on a variety of distribution shifts and publicly available backbone networks in Sec. 6.

5 Analysis

In this section, we present a theoretical analysis of PRO², aiming to understand how our proposed orthogonal feature selection procedure can lead to sample-efficient adaptation under distribution shifts. Intuitively, the more shift we can expect, the more features we should need to adapt to it, which in turn requires more samples during adaptation (to fit the features accurately). However, the choice of how we extract features influences the rate at which the sample complexity grows under distribution shift: while large shifts may still require many features, if the features are prioritized well, then smaller shifts might require only a very small number of features, and thus require fewer samples.

In our analysis, we first show that using fewer features (d) leads to lower variance, which scales as $\mathcal{O}(\sqrt{d/M})$ given M target samples, but at a cost in bias, which in some cases scales as $\mathcal{O}(\sqrt{1 - (d/D)} \cdot \text{KL}(p_S||p_T))$, which grows with the amount of shift between the source and target distributions (p_S, p_T). In Sec. 5.1, we first analyze the specific features learned by PRO² with minimal distributional assumptions. Then, in Sec. 5.2, we apply our general results to a shifted homoscedastic Gaussian (SHOG) model, where the bias and variance terms involve more intuitive terms. We also empirically verify our results using synthetic SHOG data. Additional theoretical results and proofs can be found in Appendix A.

5.1 Bias-variance tradeoffs for general shifts.

In this section, we analyze the properties of the learned projection Π on the *target distribution* to understand why PRO² may improve sample efficiency during adaptation by first extracting a set of diverse, useful features.

Probing on the target distribution. We first introduce some additional notation specific to the target distribution. For projection Π , let Π_d denote the projection matrix for $\text{span}(\{\Pi_i\}_{i=1}^d)$, i.e.,

$$\Pi_d = [\Pi_1, \dots, \Pi_d][\Pi_1, \dots, \Pi_d]^\top. \quad (1)$$

Denote the target error for classifier \mathbf{w} as $\mathcal{L}_T(\mathbf{w}) \triangleq \mathbb{E}_{p_T} l(\langle \mathbf{w}, \mathbf{x} \rangle, y)$, and the bias incurred by probing over the projected features $\text{span}(\{\Pi_i\}_{i=1}^d)$ as:

$$b_d \triangleq \min_{\mathbf{w}' \in \text{span}(\{\Pi_i\}_{i=1}^d)} \mathcal{L}_T(\mathbf{w}') - \min_{\mathbf{w} \in \mathcal{W}} \mathcal{L}_T(\mathbf{w}).$$

We also denote the d -dimensional weight vector learned by PRO² on the M projected target samples as:

$$\hat{\mathbf{w}}_d \triangleq \min_{\substack{\mathbf{w} \in \text{span}(\{\Pi_i\}_{i=1}^d) \\ \|\mathbf{w}\|_2 \leq 1}} \sum_{i=1}^M l(\langle \mathbf{w}, \mathbf{x}^{(i)} \rangle, y^{(i)}).$$

We are now ready to bound the bias b_d in Lemma 1, with a term that reduces to 0 as we add more features $d \rightarrow D$. The rate at which $b_d \rightarrow 0$ is controlled by the relationship of the optimal linear classifier on target \mathbf{w}_T^* with the projection matrix Π_d learnt on the source data. When there is no distribution shift, we know that for the projection Π_1 returned by PRO², $\Pi_1 \propto \mathbf{w}_T^*$, and thus $(\mathbf{I}_D - \Pi_1)\mathbf{w}_T^* = 0$, i.e., the bias $b_d \rightarrow 0$ with just one direction. On the other hand if Π_d is returned by a random projection then bias b_d decreases at rate $\mathcal{O}(\sqrt{1 - (d/D)})$ even when there is no distribution shift. In simpler terms, the rate at which the bias reduces as we increase d is controlled by degree of distribution shift, and how informative the source features (in Π_d) remain under this shift.

Lemma 1 (bias induced by shift). *For some \mathbf{w}_T^* that is the Bayes optimal linear predictor on distribution p_T over the full feature space, and an L -Lipschitz smooth convex loss l , the bias $b_d \leq L \cdot \|(\mathbf{I}_D - \Pi_d)\mathbf{w}_T^*\|_2$. When Π_d is a random rank d projection matrix with columns drawn uniformly over the sphere S^{d-1} , then $b_d \lesssim L \sqrt{1 - \frac{d}{D}} \cdot \|\mathbf{w}_T^*\|_2$.*

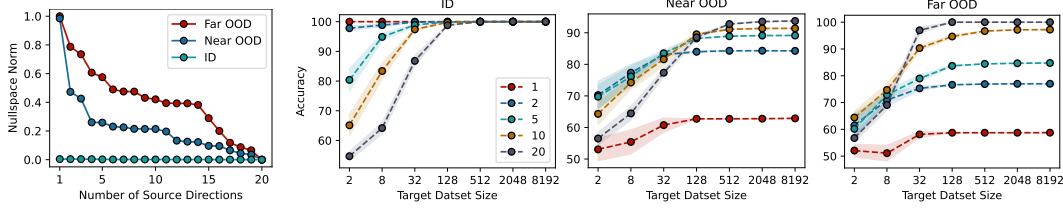


Figure 3: **Evaluation of PRO² on shifted homoscedastic Gaussian data.** (Left) The x- and y-axes denote dimensionality of A_d and nullspace norm, respectively. Nullspace norm drops slowly for more severe distribution shifts. (Right) For less severe distribution shifts (ID and Near OOD), low-dimensional projections suffer from less bias, resulting in higher accuracy in the low-data regime. For the Far OOD distribution, using all 20-dimensional features is best, as bias drops more slowly.

In Theorem 2, we describe the full bias-variance tradeoff where we see that the variance term is also controlled by the number of features d but unlike the bias is independent of the nature of shift between source and the target.

Theorem 2 (bias-variance tradeoff). *When the conditions in Lemma 1 hold and when $\|\mathbf{x}\|_\infty = \mathcal{O}(1)$, for B -bounded loss l , w.h.p. $1 - \delta$, the excess risk for the solution $\hat{\mathbf{w}}_d$ of PRO² that uses d features is $\mathcal{L}_T(\hat{\mathbf{w}}_d) - \min_{\mathbf{w} \in \mathcal{W}} \mathcal{L}_T(\mathbf{w})$*

$$\lesssim \|(I_D - \Pi_d)\mathbf{w}_T^*\|_2 + \left(\frac{\sqrt{d} + B\sqrt{\log(1/\delta)}}{\sqrt{M}} \right), \quad (2)$$

where the first term controls the bias and the second controls the variance.

This result provides insights on what factors affect generalization when probing on target data. Tighter compression of the original representation, i.e., using a smaller d , increases bias while decreasing variance. The rate of bias increase is determined by the degree of distribution shift, where more severe shifts correspond to a steeper increase in bias. However, this bias can be mitigated as long as the important features needed for prediction on the target domain are covered by the compressed representation. Thus, PRO² induces a favorable bias-variance tradeoff, as the features extracted are predictive and diverse and hence are more likely to cover the important features needed for the target domain, allowing compression to a smaller d while still maintaining low bias. The distribution shift has no effect on variance, and variance can only be decreased by using a low-dimensional represent (at the cost of bias) or learning from a larger dataset.

5.2 Bias-variance tradeoff in shifted Gaussian model.

In this subsection, we consider a simplified setting of a shifted homoscedastic Gaussian (SHOG). Within this model, we show that the more general statement in Theorem 2 can be simplified further to provide a more intuitive relationship between the factors that affect generalization. Furthermore, we empirically demonstrate the behavior predicted by our bounds on synthetic SHOG data.

Shifted homoscedastic Gaussian (SHOG) model of distribution shift. We model the source distribution as a Bernoulli mixture model of data in which binary labels are balanced ($y \sim \text{Bern}(0.5)$) and the class conditional distributions are homoscedastic multi-variate Gaussians:

$$\mathbf{x} \mid y \sim \mathcal{N}(\mu_y, \Sigma_S) \quad \text{for } y \in \{0, 1\},$$

where $\mu_1, \mu_2 \in \mathbb{R}^D$ are mean vectors and $\Sigma_S \in \mathbb{R}^{D \times D}$ is the shared covariance matrix. The target distribution has the same label distribution and Gaussian means, but a different covariance matrix given by Σ_T . We study how the relation between the two covariance matrices Σ_S, Σ_T can affect the bias term b_d when Π_d is either returned by PRO² or a random projection matrix with columns drawn uniformly over the sphere S^{d-1} .

We specialize the more general bias-variance tradeoff result to a shifted homoscedastic Gaussian (SHOG) model in Corollary 3, where we derive a simpler bound characterizing the tradeoff between performance, the value of d , and the amount of distributional shift.

Corollary 3 (tradeoff under SHOG). *Under our SHOG model of shift, and conditions for a random projection Π_d in Lemma 10, the target error $\mathcal{L}_T(\hat{\mathbf{w}}_d) \lesssim \mathcal{O}\left(\sqrt{1 - \frac{d}{D}} \cdot \text{KL}(p_S||p_T)\right) + \sqrt{\frac{d}{M}}$, when $\|\Sigma_T\|_{\text{op}} = O(1)$.*

In Fig. 3, we plot the nullspace norm $\|\Sigma_S\|_{\text{op}}$ for different d in three target distributions of varying distribution shift severity in the SHOG model. We see that the more severe shifts have a higher norm, indicating that the OOD distributions suffer from high bias when d is low. Indeed, we see that the ID distribution suffers from virtually no bias, making $d = 1$ achieve highest target accuracy for all dataset sizes. In contrast, the Near OOD and Far OOD distributions suffer from high bias of up to 40% accuracy, and higher projection dimension d is needed for adaptation, as predicted by Corollary 3.

6 Experiments

In this section, we aim to empirically answer the following questions: (1) Can PRO² identify a feature-space basis for rapid adaptation, and how does it compare to other methods for extracting features? (2) How does the dimensionality of the feature-space basis affect sample efficiency in different distribution shift conditions? We provide additional empirical results and analyses, such as showing that the adaptation performance of PRO² improves with better pre-trained backbones, in Appendix C. Details on pre-trained models and training details are in Appendix B.

6.1 Experimental Setup

Datasets. We run experiments on six datasets with distribution shifts: 4-way collages [51], Waterbirds [44], CelebA [32], Camelyon [4], Living17 [45], and FMoW [22] datasets. Each of these datasets have a source distribution that we use for training. For the first four datasets, we construct multiple target distributions for evaluation, representative of a range of potential test distributions. For the latter two datasets, which are larger datasets representing shifts that may occur in the wild, we evaluate on the given test set. For all settings, we use the original source datasets, which each contain thousands of datapoints. For target data, we subsample very small label-balanced datasets for adaptation, with $\{2, 8, 32, 128\}$ images per label for the first four datasets and $\{1, 2, 5\}$ images per label for the latter two datasets. The remaining target distribution datapoints are used for evaluation. Due to space constraints, we describe the different target distributions in Appendix B.

Computational efficiency. Similarly to Mehta et al. [36], we use feature embeddings from a pre-trained backbone without fine-tuning. Our aim is to develop methods that can leverage pretrained models out-of-the-box with minimal computational requirements: our training involves at most two linear layers on top of cached feature vectors. For all comparisons, we hyperparameter tune over 3 different learning rates (0.1, 0.01, and 0.001) as well as 3 different L_2 regularization weights (0.1, 0.01, 0.001). In our main experiments in Sec. 6.2, we also sweep over 6 different projection dimensions ($d = 1, 4, 16, 64, 256, 1024$) and report results over 10 runs. For hyperparameter tuning, we adopt the typical practice of using a target validation set, which is common in prior work in similar transfer learning settings [21, 36, 26]. The challenge of hyperparameter tuning for a target domain without additional domain-specific information remains an open problem that we hope can be addressed in future work. As a demonstration of the computational efficiency of PRO², after caching pre-trained embeddings, we can collectively run all experiments in Sec. 6.2, which is nearly 30k runs due to hyperparameter tuning, within 24 hours using four standard CPUs and *no GPUs*. We find that PRO² is robust to learning rate, which is expected as the optimization problem is linear.

6.2 Comparison to prior projection methods

We investigate whether PRO² can extract features that can facilitate adaptation to different distribution shifts, and how it compares other feature extraction methods. We perform a comprehensive experimental evaluation on the six datasets, comparing PRO² against four other projection methods: (1) Random Projection, (2) DFR [21], which uses standard linear probing, and (3) Teney et al. [51], which aims to learn multiple predictive patterns by minimizing the alignment of input gradients over pairs of features. Experiments in Fig. 4 and Tab. 1 indicate that across all different target distributions six datasets, PRO² significantly outperforms Random Projection and DFR, especially in the low-data regime. In particular, these results show that DFR or standard linear probing, the strategy

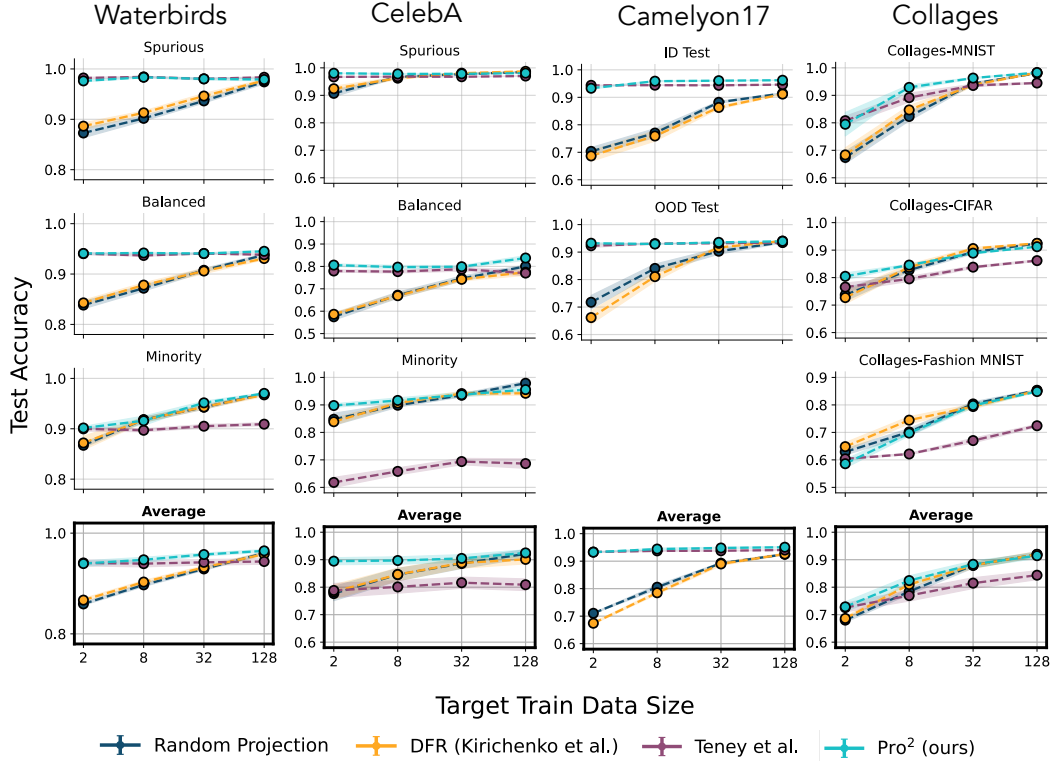


Figure 4: **Main results.** We compare 4 different methods for learning features to adapt to a target distribution: (1) Random Projection, (2) DFR [21], (3) Teney et al. [51], and (4) PRO^2 . We report average target accuracies after probing with different target dataset sizes ranging from 2 to 128 datapoints per label; error bars indicate standard error across 10 runs. PRO^2 is the best performing or tied for best performing method *across each of these 4 datasets with any amount of target data*. PRO^2 substantially outperforms Random Projection and DFR in the low-data regime on all four datasets. PRO^2 also outperforms Teney et al. [51] on average on 3 of the 4 datasets particularly when given more target data.

Target Train Data Size (per label)	Living17			FMoW		
	1	2	5	1	2	5
Random Projection	85.7 (0.6)	92.7 (1.0)	99.2 (0.1)	16.3 (0.7)	23.6 (0.6)	33.3 (0.6)
DFR (Kirichenko et al.)	87.1 (0.9)	95.0 (0.9)	98.8 (0.3)	17.5 (0.8)	24.0 (0.6)	35.1 (0.6)
PRO^2	91.2 (0.4)	95.7 (0.7)	99.2 (0.06)	20.2 (0.9)	28.7 (1.1)	37.2 (0.8)

Table 1: **Additional main results.** We run additional experiments on the Living17 dataset from the Breeds benchmark [45] and FMoW [22], reporting adaptation accuracy and standard error across 10 runs. Both of these datasets are challenging multi-class distribution shift tasks and are representative of real-world scenarios. We find that similar to the other datasets, PRO^2 is the best performing or tied for best performing method on these datasets when given a limited amount of target data.

adopted by several additional prior works by default [36, 19], is not the most data-efficient way to utilize pre-trained embeddings when given limited target data. This is because such embeddings contain redundant or non-predictive information, and including these features during adaptation leads to higher variance without decreasing bias, which in turn means that we need more labeled samples. In contrast, PRO^2 improves sample efficiency by first extracting a predictive feature-space basis from the source distribution, removing redundant information. Teney et al. [51] is sufficient in some scenarios with milder distribution shift, where a diverse range of features are not needed for adaptation. However, it fails to achieve high accuracy given a large target dataset on more severe distribution shifts, such as the Minority distributions on Waterbirds and CelebA or the Fashion-MNIST and CIFAR distributions in 4-Way Collages. This indicates that the feature diversity from the orthogonality constraint gives PRO^2 better coverage of different features, enabling better adaptation to severe distribution shifts given enough target data. These results demonstrate the effectiveness of PRO^2 compared to existing methods in the few-shot adaptation problem setting.

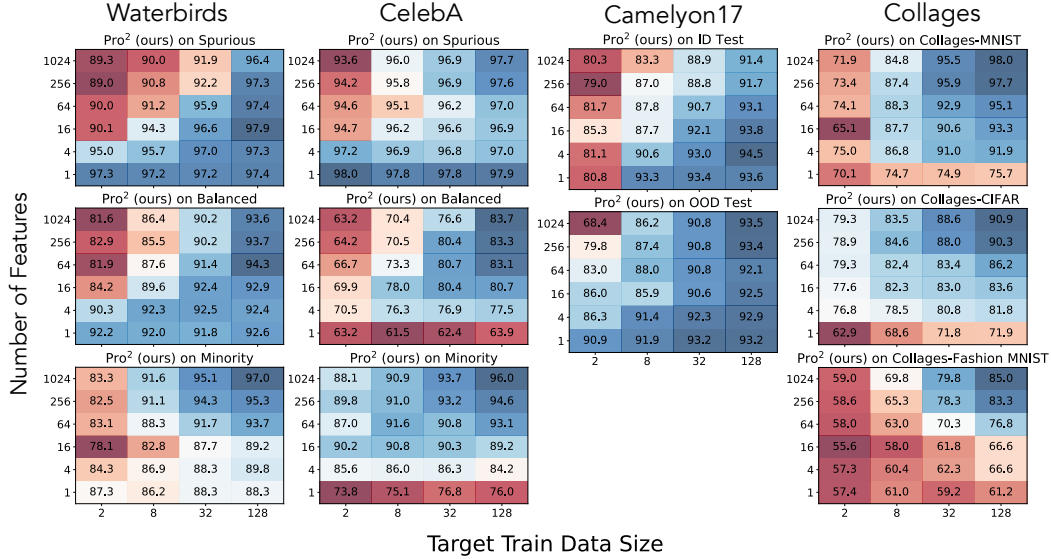


Figure 5: **Feature-space dimensionality of PRO^2 and severity of distribution shift.** We vary the feature-space dimensions d (y-axis) of PRO^2 and report held-out accuracy after training on target datasets of different size (x-axis) on our 4 datasets. Higher accuracies are in blue and lower accuracies are in red. We see that smaller feature-space dimensions suffice for target distributions with milder distribution shifts while higher dimensions are required for more severe shifts. For example, on the spurious test distribution (small dist. shift) of Waterbirds/CelebA, the bottom row, which uses $d = 1$ is bluest, while the blue is concentrated in the top right squares (which use more features and more data) for more difficult distribution shifts such as Minority for Waterbirds/CelebA and the collages test sets.

6.3 Projection dimension and shift severity

In this subsection, we investigate how the feature-space dimension d affects the sample efficiency of PRO^2 , for different degrees of distribution shift. Experiments in Fig. 5 show that when the distribution shift is less severe, such as the Spurious test distributions on Waterbirds and CelebA, it is helpful to reduce the number of features used. This scenario is analogous to the ID setting in Fig. 3. In such scenarios, the top-ranked features from the source data are also predictive on the target distribution, and incorporating additional features worsens generalization because it increases variance without sufficiently decreasing bias. However, when the distribution shift is more severe, such as the Minority distributions on Waterbirds and CelebA or Collages-Fashion MNIST and Collages-CIFAR, it is helpful to increase the number of features used. This scenario is analogous to the Far OOD setting in Fig. 3. These empirical results are supported formally by our theoretical results in Sec. 5, which show that the optimal number of features to use increases with distribution shift severity.

7 Conclusion

In this paper, we propose PRO^2 , a lightweight framework consisting of 2 steps: (1) a projection step that extracts a diverse and predictive feature-space basis and (2) a probing step that interpolates between the projected features to efficiently adapt varying target distributions. Our theoretical and empirical analyses reveal a number of interesting novel insights: (i) standard linear probing is not the best approach for few-shot adaptation; (ii) Retaining a diverse range of potentially useful features that different target distributions may require improves sample efficiency, (iii) we can trade off how much to adapt (size of the feature-space basis) vs number of samples, picking the best basis to adapt for each level of shift. These insights open up a range of exciting paths for future work. First, our framework may be extended to other problem settings, such as the active learning setting, in which the model can adaptively request target labels. Another interesting direction is developing methods to better determine the optimal number of features and best feature basis to use when adapting. Integrating PRO^2 with other fine-tuning methods is also a promising direction for further improving adaptation performance. Finally, another interesting direction would be selecting which features to use in an unsupervised fashion, without any labeled target data.

Acknowledgments

We thank members of the IRIS and RAIL labs for helpful discussions on this project. This work was supported by NSF, KFAS, Apple, Juniper, and ONR grant N00014-20-1-2675.

References

- [1] Alemi, A. A., Fischer, I., Dillon, J. V., and Murphy, K. (2016). Deep variational information bottleneck. *arXiv preprint arXiv:1612.00410*.
- [2] Arjovsky, M., Bottou, L., Gulrajani, I., and Lopez-Paz, D. (2019). Invariant risk minimization. *arXiv preprint arXiv:1907.02893*.
- [3] Arpit, D., Jastrzebski, S., Ballas, N., Krueger, D., Bengio, E., Kanwal, M. S., Maharaj, T., Fischer, A., Courville, A., Bengio, Y., et al. (2017). A closer look at memorization in deep networks. In *International Conference on Machine Learning*.
- [4] Bandi, P., Geessink, O., Manson, Q., Van Dijk, M., Balkenhol, M., Hermesen, M., Bejnordi, B. E., Lee, B., Paeng, K., Zhong, A., et al. (2018). From detection of individual metastases to classification of lymph node status at the patient level: the camelyon17 challenge. *IEEE Transactions on Medical Imaging*.
- [5] Bartlett, P. L. and Mendelson, S. (2002). Rademacher and gaussian complexities: Risk bounds and structural results. *Journal of Machine Learning Research*, 3(Nov):463–482.
- [6] Caron, M., Misra, I., Mairal, J., Goyal, P., Bojanowski, P., and Joulin, A. (2020). Unsupervised learning of visual features by contrasting cluster assignments. *Advances in Neural Information Processing Systems*, 33:9912–9924.
- [7] Chandrashekar, G. and Sahin, F. (2014). A survey on feature selection methods. *Computers & Electrical Engineering*, 40(1):16–28.
- [8] Creager, E., Jacobsen, J.-H., and Zemel, R. (2021). Environment inference for invariant learning. In *International Conference on Machine Learning*.
- [9] Cunningham, J. P. and Ghahramani, Z. (2015). Linear dimensionality reduction: Survey, insights, and generalizations. *The Journal of Machine Learning Research*, 16(1):2859–2900.
- [10] Dash, M. and Liu, H. (1997). Feature selection for classification. *Intelligent data analysis*, 1(1-4):131–156.
- [11] Dosovitskiy, A., Beyer, L., Kolesnikov, A., Weissenborn, D., Zhai, X., Unterthiner, T., Dehghani, M., Minderer, M., Heigold, G., Gelly, S., et al. (2020). An image is worth 16x16 words: Transformers for image recognition at scale. *arXiv preprint arXiv:2010.11929*.
- [12] Fisher, A., Rudin, C., and Dominici, F. (2019). All models are wrong, but many are useful: Learning a variable’s importance by studying an entire class of prediction models simultaneously. *J. Mach. Learn. Res.*, 20(177):1–81.
- [13] Gandelsman, Y., Sun, Y., Chen, X., and Efros, A. A. (2022). Test-time training with masked autoencoders. *arXiv preprint arXiv:2209.07522*.
- [14] Ganin, Y., Ustinova, E., Ajakan, H., Germain, P., Larochelle, H., Laviolette, F., Marchand, M., and Lempitsky, V. (2016). Domain-adversarial training of neural networks. *The journal of machine learning research*, 17(1):2096–2030.
- [15] Geirhos, R., Jacobsen, J.-H., Michaelis, C., Zemel, R., Brendel, W., Bethge, M., and Wichmann, F. A. (2020). Shortcut learning in deep neural networks. *Nature Machine Intelligence*, 2(11):665–673.
- [16] Gunasekar, S., Lee, J. D., Soudry, D., and Srebro, N. (2018). Implicit bias of gradient descent on linear convolutional networks. In Bengio, S., Wallach, H., Larochelle, H., Grauman, K., Cesa-Bianchi, N., and Garnett, R., editors, *Advances in Neural Information Processing Systems*.

- [17] He, K., Zhang, X., Ren, S., and Sun, J. (2016). Deep residual learning for image recognition. In *Proceedings of the IEEE conference on computer vision and pattern recognition*, pages 770–778.
- [18] Iwasawa, Y. and Matsuo, Y. (2021). Test-time classifier adjustment module for model-agnostic domain generalization. *Advances in Neural Information Processing Systems*, 34:2427–2440.
- [19] Izmailov, P., Kirichenko, P., Gruver, N., and Wilson, A. G. (2022). On feature learning in the presence of spurious correlations. *arXiv preprint arXiv:2210.11369*.
- [20] Kakade, S. M., Sridharan, K., and Tewari, A. (2008). On the complexity of linear prediction: Risk bounds, margin bounds, and regularization. *Advances in neural information processing systems*, 21.
- [21] Kirichenko, P., Izmailov, P., and Wilson, A. G. (2022). Last layer re-training is sufficient for robustness to spurious correlations. *arXiv preprint arXiv:2204.02937*.
- [22] Koh, P. W., Sagawa, S., Xie, S. M., Zhang, M., Balsubramani, A., Hu, W., Yasunaga, M., Phillips, R. L., Gao, I., Lee, T., et al. (2021). Wilds: A benchmark of in-the-wild distribution shifts. In *International Conference on Machine Learning*, pages 5637–5664. PMLR.
- [23] Kornblith, S., Shlens, J., and Le, Q. (2018). Do better imagenet models transfer better? arxiv 2018. *arXiv preprint arXiv:1805.08974*.
- [24] Kumar, A., Raghunathan, A., Jones, R., Ma, T., and Liang, P. (2022). Fine-tuning can distort pretrained features and underperform out-of-distribution. *arXiv preprint arXiv:2202.10054*.
- [25] Lee, J. A., Verleysen, M., et al. (2007). *Nonlinear dimensionality reduction*, volume 1. Springer.
- [26] Lee, Y., Chen, A. S., Tajwar, F., Kumar, A., Yao, H., Liang, P., and Finn, C. (2022a). Surgical fine-tuning improves adaptation to distribution shifts. *arXiv preprint arXiv:2210.11466*.
- [27] Lee, Y., Yao, H., and Finn, C. (2022b). Diversify and disambiguate: Learning from underspecified data. *arXiv preprint arXiv:2202.03418*.
- [28] Li, J., Cheng, K., Wang, S., Morstatter, F., Trevino, R. P., Tang, J., and Liu, H. (2017). Feature selection: A data perspective. *ACM computing surveys (CSUR)*, 50(6):1–45.
- [29] Li, Z., Evtimov, I., Gordo, A., Hazirbas, C., Hassner, T., Ferrer, C. C., Xu, C., and Ibrahim, M. (2022). A whac-a-mole dilemma: Shortcuts come in multiples where mitigating one amplifies others.
- [30] Liu, E. Z., Haghighi, B., Chen, A. S., Raghunathan, A., Koh, P. W., Sagawa, S., Liang, P., and Finn, C. (2021). Just train twice: Improving group robustness without training group information. In *International Conference on Machine Learning*, pages 6781–6792. PMLR.
- [31] Liu, H. and Motoda, H. (2007). *Computational methods of feature selection*. CRC press.
- [32] Liu, Z., Luo, P., Wang, X., and Tang, X. (2015). Deep learning face attributes in the wild. In *Proceedings of International Conference on Computer Vision (ICCV)*.
- [33] Loshchilov, I. and Hutter, F. (2017). Decoupled weight decay regularization. *arXiv preprint arXiv:1711.05101*.
- [34] Lubana, E. S., Bigelow, E. J., Dick, R. P., Krueger, D., and Tanaka, H. (2022). Mechanistic mode connectivity. *arXiv preprint arXiv:2211.08422*.
- [35] May, A., Zhang, J., Dao, T., and Ré, C. (2019). On the downstream performance of compressed word embeddings. In Wallach, H., Larochelle, H., Beygelzimer, A., d’Alché-Buc, F., Fox, E., and Garnett, R., editors, *Advances in Neural Information Processing Systems*, volume 32. Curran Associates, Inc.
- [36] Mehta, R., Albiero, V., Chen, L., Evtimov, I., Glaser, T., Li, Z., and Hassner, T. (2022). You only need a good embeddings extractor to fix spurious correlations.

- [37] Morwani, D., Batra, J., Jain, P., and Netrapalli, P. (2023). Simplicity bias in 1-hidden layer neural networks. *arXiv preprint arXiv:2302.00457*.
- [38] Nam, J., Cha, H., Ahn, S., Lee, J., and Shin, J. (2020). Learning from failure: Training debiased classifier from biased classifier. *Conference on Neural Information Processing Systems*.
- [39] Oquab, M., Bottou, L., Laptev, I., and Sivic, J. (2014). Learning and transferring mid-level image representations using convolutional neural networks. In *Proceedings of the IEEE conference on computer vision and pattern recognition*, pages 1717–1724.
- [40] Pagliardini, M., Jaggi, M., Fleuret, F., and Karimireddy, S. P. (2022). Agree to disagree: Diversity through disagreement for better transferability. *arXiv preprint arXiv:2202.04414*.
- [41] Petridis, S. and Perantonis, S. J. (2004). On the relation between discriminant analysis and mutual information for supervised linear feature extraction. *Pattern Recognition*, 37(5):857–874.
- [42] Pezeshki, M., Kaba, S.-O., Bengio, Y., Courville, A., Precup, D., and Lajoie, G. (2021). Gradient starvation: A learning proclivity in neural networks. In Beygelzimer, A., Dauphin, Y., Liang, P., and Vaughan, J. W., editors, *Advances in Neural Information Processing Systems*.
- [43] Rosenfeld, E., Ravikumar, P., and Risteski, A. (2022). Domain-adjusted regression or: Erm may already learn features sufficient for out-of-distribution generalization. *arXiv preprint arXiv:2202.06856*.
- [44] Sagawa, S., Koh, P. W., Hashimoto, T. B., and Liang, P. (2020). Distributionally robust neural networks for group shifts: On the importance of regularization for worst-case generalization. *International Conference on Learning Representations*.
- [45] Santurkar, S., Tsipras, D., and Madry, A. (2020). Breeds: Benchmarks for subpopulation shift. *arXiv preprint arXiv:2008.04859*.
- [46] Semenova, L., Rudin, C., and Parr, R. (2019). A study in rashomon curves and volumes: A new perspective on generalization and model simplicity in machine learning. *arXiv preprint arXiv:1908.01755*.
- [47] Shah, H., Tamuly, K., Raghunathan, A., Jain, P., and Netrapalli, P. (2020). The pitfalls of simplicity bias in neural networks. *Conference on Neural Information Processing Systems*.
- [48] Sharif Razavian, A., Azizpour, H., Sullivan, J., and Carlsson, S. (2014). Cnn features off-the-shelf: an astounding baseline for recognition. In *Proceedings of the IEEE conference on computer vision and pattern recognition workshops*, pages 806–813.
- [49] Sorzano, C. O. S., Vargas, J., and Montano, A. P. (2014). A survey of dimensionality reduction techniques. *arXiv preprint arXiv:1403.2877*.
- [50] Sun, Y., Wang, X., Liu, Z., Miller, J., Efros, A., and Hardt, M. (2020). Test-time training with self-supervision for generalization under distribution shifts. In *International conference on machine learning*, pages 9229–9248. PMLR.
- [51] Teney, D., Abbasnejad, E., Lucey, S., and Hengel, A. v. d. (2021). Evading the simplicity bias: Training a diverse set of models discovers solutions with superior ood generalization. *arXiv preprint arXiv:2105.05612*.
- [52] Teney, D., Abbasnejad, E., Lucey, S., and van den Hengel, A. (2022). Evading the simplicity bias: Training a diverse set of models discovers solutions with superior ood generalization. In *Proceedings of the IEEE/CVF Conference on Computer Vision and Pattern Recognition*, pages 16761–16772.
- [53] Tishby, N., Pereira, F. C., and Bialek, W. (2000). The information bottleneck method. *arXiv preprint physics/0004057*.
- [54] Tzeng, E., Hoffman, J., Zhang, N., Saenko, K., and Darrell, T. (2014). Deep domain confusion: Maximizing for domain invariance. *arXiv preprint arXiv:1412.3474*.

- [55] Varsavsky, T., Orbes-Arteaga, M., Sudre, C. H., Graham, M. S., Nachev, P., and Cardoso, M. J. (2020). Test-time unsupervised domain adaptation. In *International Conference on Medical Image Computing and Computer-Assisted Intervention*, pages 428–436. Springer.
- [56] Wainwright, M. J. (2019). *High-dimensional statistics: A non-asymptotic viewpoint*, volume 48. Cambridge university press.
- [57] Wang, D., Shelhamer, E., Liu, S., Olshausen, B., and Darrell, T. (2020). Tent: Fully test-time adaptation by entropy minimization. *arXiv preprint arXiv:2006.10726*.
- [58] Wortsman, M., Ilharco, G., Kim, J. W., Li, M., Kornblith, S., Roelofs, R., Lopes, R. G., Hajishirzi, H., Farhadi, A., Namkoong, H., and Schmidt, L. (2022). Robust fine-tuning of zero-shot models. In *Proceedings of the IEEE/CVF Conference on Computer Vision and Pattern Recognition (CVPR)*, pages 7959–7971.
- [59] Xu, Y., He, H., Shen, T., and Jaakkola, T. (2022). Controlling directions orthogonal to a classifier. *arXiv preprint arXiv:2201.11259*.
- [60] Yosinski, J., Clune, J., Bengio, Y., and Lipson, H. (2014). How transferable are features in deep neural networks? *Advances in neural information processing systems*, 27.
- [61] Zhai, X., Puigcerver, J., Kolesnikov, A., Ruysen, P., Riquelme, C., Lucic, M., Djolonga, J., Pinto, A. S., Neumann, M., Dosovitskiy, A., et al. (2019). A large-scale study of representation learning with the visual task adaptation benchmark. *arXiv preprint arXiv:1910.04867*.
- [62] Zhang, M., Marklund, H., Dhawan, N., Gupta, A., Levine, S., and Finn, C. (2021). Adaptive risk minimization: Learning to adapt to domain shift. *Advances in Neural Information Processing Systems*, 34:23664–23678.
- [63] Zhang, M. and Ré, C. (2022). Contrastive adapters for foundation model group robustness. *arXiv preprint arXiv:2207.07180*.

A Proofs for Theoretical Analysis

We present proofs for our theoretical analysis in Sec. 5 along with some additional statements. As in the main paper, we denote the dimensionality of the feature-space basis learned by PRO² as d , the original dimension of the representations given by the feature backbone f as D , source and target distributions as p_S and p_T , and the number of source and target datapoints as N and M . We let Π_d denote the projection matrix for $\text{span}(\{\Pi_i\}_{i=1}^d)$, i.e., $\Pi_d = [\Pi_1, \dots, \Pi_d][\Pi_1, \dots, \Pi_d]^\top$. If the target error for the feature w is $\mathcal{L}_T(\mathbf{w}) := \mathbb{E}_{\mathcal{D}_T} l(\langle \mathbf{w}, \mathbf{x} \rangle, y)$, then the bias incurred by probing on the subspace Π_d consisting of source features is:

$$b_d := \min_{\mathbf{w}' \in \text{span}(\{\Pi_i\}_{i=1}^d)} \mathcal{L}_T(\mathbf{w}') - \min_{\mathbf{w} \in \mathcal{W}} \mathcal{L}_T(\mathbf{w}),$$

and we denote the feature-space basis of dimensionality d learned by PRO² as follows:

$$\hat{\mathbf{w}}_d := \arg \min_{\mathbf{w} \in \text{span}(\{\Pi_i\}_{i=1}^d)} \sum_{i=1}^M l(\langle \mathbf{w}, \mathbf{x}^{(i)} \rangle, y^{(i)}). \quad (3)$$

From the original D -dimensional feature representations given by our feature backbone f , we want our learned linear projections $\Pi : \mathbb{R}^D \rightarrow \mathbb{R}^d$ to retain as much information as possible that is relevant in predicting the label y . In other words, we want to maximize the mutual information between the projected features $\Pi(\mathbf{x})$ and the labels y . In Theorem 6, We first formally characterize the solution found by the projection step in PRO² as maximizing this mutual information amongst all rank d matrices with orthogonal columns, using the following two lemmas.

Lemma 4 (Entropy of a sub-gaussian under low rank projection). *For a σ -sub-gaussian random variable \mathbf{x} , and rank r orthonormal matrix $\mathbf{A} \in \mathbb{R}^{d \times D}$ the differential entropy $H(\mathbf{A}\mathbf{x})$ for projection $\mathbf{A}\mathbf{x}$ is $\mathcal{O}(1/d)$ when $\log \sigma = \mathcal{O}(1/d^2)$.*

Proof. Let \mathbf{A}_i denote the i^{th} row of \mathbf{A} , then:

$$H(\mathbf{A}\mathbf{x}) = H([\mathbf{A}_1^\top \mathbf{x}, \dots, \mathbf{A}_r^\top \mathbf{x}]^\top) = H(\mathbf{A}_1^\top \mathbf{x}) + \sum_{i=2}^r H(\mathbf{A}_i^\top \mathbf{x} \mid \mathbf{A}_1^\top \mathbf{x}, \dots, \mathbf{A}_{i-1}^\top \mathbf{x}) \leq \sum_{i=1}^r H(\mathbf{A}_i^\top \mathbf{x})$$

Since, \mathbf{x} is σ -sub-gaussian, using standard bounds on differential entropy and the inequality above we can argue that:

$$\begin{aligned} \mathbb{E} \left[e^{t^2 \mathbf{A}_i^\top \mathbf{x}} \right] &\leq e^{t^2 \sigma^2 / 2}, \quad \forall i, t \\ \implies H(\mathbf{A}_i^\top \mathbf{x}) &\leq \frac{1}{2} \log(2\pi e \sigma^2) \quad \forall i \\ \implies H(\mathbf{A}_i^\top \mathbf{x}) &\lesssim (1/d^2) \quad \forall i \quad (\text{since } \log \sigma = \mathcal{O}(1/d^2)) \\ \implies H(\mathbf{A}\mathbf{x}) &= \mathcal{O}(1/d) \end{aligned}$$

□

Lemma 5 (Entropy for a mixture of σ -sub-gaussians). *For a d -dimensional random variable \mathbf{x} that is a mixture of two σ -sub-gaussian random variables \mathbf{x}_1 and \mathbf{x}_2 with overlapping supports, bounded Jensen-Shannon divergence $\text{JS}(\mathbf{v}^\top \mathbf{x}_1 \parallel \mathbf{v}^\top \mathbf{x}_2) \leq \beta$ and mixture proportion $\alpha \in [0, 1]$ i.e., the density function $p(\mathbf{x}) = \alpha \cdot p_1(\mathbf{x}) + (1 - \alpha) \cdot p_2(\mathbf{x})$, then the entropy $H(\mathbf{v}^\top \mathbf{x})$ for $\|\mathbf{v}\|_2 = 1$, is at most $\mathcal{O}(\log \sigma + \beta)$.*

Proof. Using Jensen inequality and the definition of KL divergence, the differential entropy can be broken down as follows:

$$\begin{aligned} H(\mathbf{v}^\top \mathbf{x}) &= - \int (\alpha \cdot p_1(\mathbf{v}^\top \mathbf{x}) + (1 - \alpha) \cdot p_2(\mathbf{v}^\top \mathbf{x})) \log(\alpha \cdot p_1(\mathbf{v}^\top \mathbf{x}) + (1 - \alpha) \cdot p_2(\mathbf{v}^\top \mathbf{x})) d\mathbf{x} \\ &\leq \alpha^2 H(\mathbf{v}^\top \mathbf{x}_1) + (1 - \alpha)^2 H(\mathbf{v}^\top \mathbf{x}_2) \\ &\quad - \alpha(1 - \alpha) \int p_1(\mathbf{v}^\top \mathbf{x}) \log p_2(\mathbf{v}^\top \mathbf{x}) d\mathbf{x} - \alpha(1 - \alpha) \int p_2(\mathbf{v}^\top \mathbf{x}) \log p_1(\mathbf{v}^\top \mathbf{x}) d\mathbf{x} \\ &\leq \alpha H(\mathbf{v}^\top \mathbf{x}_1) + (1 - \alpha) H(\mathbf{v}^\top \mathbf{x}_2) + 2\alpha(1 - \alpha)\beta \\ &\lesssim \log(\sigma) + \beta \end{aligned}$$

where the last step follows from the first two arguments made in the proof for Lemma 4. □

Theorem 6 (Information in projected input). *When the distributions $p(\mathbf{x} \mid y)$ are $\exp(d^{-2})$ -sub-gaussian for each y and the Jensen-Shannon divergence $\text{JS}(p(\mathbf{v}^\top \mathbf{x} \mid y = 0) \parallel p(\mathbf{v}^\top \mathbf{x} \mid y = 1)) = \mathcal{O}(1/d)$, the solution $\{\Pi_i\}_{i=1}^d$ returned by PRO² maximizes a tight lower bound (difference bounded by an $\mathcal{O}(1)$ constant) on the mutual information criterion $I(\mathbf{A}\mathbf{x}; y)$ among all $d \times D$ row-orthonormal matrices \mathbf{A} . (See end of the proof for **discussion on assumptions** and **remark on tightness**).*

Proof. We use an inductive argument on d . Consider the following maximization problem where \mathbb{B}_d is the set of all row orthonormal matrices of row rank $d \ll D$:

$$\max_{\mathbf{A} \in \mathbb{B}_d} I(\mathbf{A}\mathbf{x}; y). \quad (4)$$

Let $d > 1$. Then, we can re-write the above as:

$$\max_{\mathbf{A} \in \mathbb{B}^{d \times D}} I(\mathbf{A}\mathbf{x}; y) = \max_{\mathbf{A}' \in \mathbb{B}_{d-1}, \mathbf{v} \in \mathbb{R}^D} I\left([\mathbf{A}'\mathbf{x}, \mathbf{v}^\top \mathbf{x}]^\top; y\right) \quad \text{where, } \mathbf{v} \in \text{NullSpace}(\mathbf{A}'), \|\mathbf{v}\|_2 = 1. \quad (5)$$

Now, we can decompose this expression using the conditional mutual information identities:

$$\begin{aligned} I\left([\mathbf{A}'\mathbf{x}, \mathbf{v}^\top \mathbf{x}]^\top; y\right) &= I(\mathbf{A}'\mathbf{x}; y) + I(\mathbf{v}^\top \mathbf{x}; y) - I(\mathbf{v}^\top \mathbf{x}; \mathbf{A}'\mathbf{x}) + I(\mathbf{v}^\top \mathbf{x}; \mathbf{A}'\mathbf{x} \mid y) \\ &= I(\mathbf{A}'\mathbf{x}; y) + I(\mathbf{v}^\top \mathbf{x}; y) - (I(\mathbf{v}^\top \mathbf{x}; \mathbf{A}'\mathbf{x}) - I(\mathbf{v}^\top \mathbf{x}; \mathbf{A}'\mathbf{x} \mid y)) \end{aligned} \quad (6)$$

Now, we upper bound the drop in information when we condition on y : $(I(\mathbf{v}^\top \mathbf{x}; \mathbf{A}'\mathbf{x}) - I(\mathbf{v}^\top \mathbf{x}; \mathbf{A}'\mathbf{x} \mid y))$ using Lemma 4 and Lemma 5.

$$\begin{aligned} I(\mathbf{v}^\top \mathbf{x}; \mathbf{A}'\mathbf{x}) - I(\mathbf{v}^\top \mathbf{x}; \mathbf{A}'\mathbf{x} \mid y) &= H([\mathbf{v}^\top \mathbf{x}; \mathbf{A}'\mathbf{x}]^\top \mid y) - H(\mathbf{v}^\top \mathbf{x} \mid y) - H(\mathbf{A}'\mathbf{x} \mid y) + I(\mathbf{v}^\top \mathbf{x}; \mathbf{A}'\mathbf{x}) \\ &\leq H([\mathbf{v}^\top \mathbf{x}; \mathbf{A}'\mathbf{x}]^\top \mid y) + H(\mathbf{v}^\top \mathbf{x}) = H(\mathbf{A}\mathbf{x} \mid y) + H(\mathbf{v}^\top \mathbf{x}) \\ &\lesssim \log \sigma + \beta = \mathcal{O}(1/d), \end{aligned} \quad (7)$$

where the last statement applies Lemma 4 to bound $H(\mathbf{A}\mathbf{x} \mid y)$ (since $\mathbf{A}\mathbf{x} \mid y = 0$ and $\mathbf{A}\mathbf{x} \mid y = 1$ are σ -sub-gaussian) and Lemma 5 to bound the entropy on the mixture of sub-gaussians $H(\mathbf{v}^\top \mathbf{x})$. Also, note that the conditional distributions differ in Jensen-Shannon divergence by $\mathcal{O}(1/d)$ and the sub-gaussian assumption gives us $\log \sigma = \mathcal{O}(1/d^2)$.

Using equation 6, equation 7 we have:

$$\max_{\mathbf{A} \in \mathbb{B}_d} I(\mathbf{A}\mathbf{x}; y) \geq \max_{\substack{\mathbf{A}' \in \mathbb{B}_{d-1}, \\ \mathbf{v} \in \text{NullSpace}(\mathbf{A}'), \|\mathbf{v}\|_2=1}} I(\mathbf{A}'\mathbf{x}; y) + I(\mathbf{v}^\top \mathbf{x}; y) - \mathcal{O}(1/d). \quad (8)$$

Let \mathbf{A}_i denote the i^{th} row of \mathbf{A} , then. Then, applying the above inductively for all d :

$$\max_{\mathbf{A} \in \mathbb{B}_d} I(\mathbf{A}\mathbf{x}; y) \geq \max_{\mathbf{A} \in \mathbb{B}_d} \left(\sum_{i=1}^{i=d} I(\mathbf{A}_i^\top \mathbf{x}; y) \right) - \mathcal{O}(1) \quad (9)$$

Let \mathbf{A}^* be the solution of the right hand side and $\mathbf{v}^* = \arg \max_{\mathbf{v}: \|\mathbf{v}\|_2=1} I(\mathbf{v}^\top \mathbf{x}; y)$. Next, we note that $\exists i$ such that $\mathbf{A}_i^* = \mathbf{v}^*$. It is easy to prove this by contradiction. Consider the case where $\nexists i$ such that $\mathbf{A}_i^* = \mathbf{v}^*$. Then, we can construct a solution $\{(\mathbf{I}_D - \mathbf{v}^* \mathbf{v}^{*\top}) \mathbf{A}_i^*\}_{i=1}^d$, order them by mutual information $I((\mathbf{A}_i^*)^\top (\mathbf{I}_D - \mathbf{v}^* \mathbf{v}^{*\top}) \mathbf{x}; y)$, take the top $d-1$ entries and append to this set \mathbf{v}^* . The new solution would have a higher value of the objective on the right hand side of equation 9, since the new solution retains optimal directions perpendicular to \mathbf{v}^* while adding \mathbf{v}^* to the set. Thus, we arrive at a contradiction and it is clear that \mathbf{v}^* belongs to the solution \mathbf{A}^* for the objective on the right side of equation 9.

Knowing that \mathbf{v}^* has to be part of \mathbf{A}^* , we can now write the right side of equation 9 as the following:

$$\begin{aligned} \max_{\mathbf{A} \in \mathbb{R}^{d \times D}} I(\mathbf{A}\mathbf{x}; y) &\geq \max_{\mathbf{v}_1 \in \mathbb{R}^D} I(\mathbf{v}_1^\top \mathbf{x}; y) \\ &\quad + \max_{\mathbf{v}_2 \in \mathbb{R}^D} I\left(\mathbf{v}_2^\top \left(\mathbf{I} - \mathbf{v}_1^* \mathbf{v}_1^{*\top}\right) \mathbf{x}; y\right) \\ &\quad + \max_{\mathbf{v}_3 \in \mathbb{R}^D} I\left(\mathbf{v}_3^\top \left(\mathbf{I} - \mathbf{v}_2^* \mathbf{v}_2^{*\top}\right) \left(\mathbf{I} - \mathbf{v}_1^* \mathbf{v}_1^{*\top}\right) \mathbf{x}; y\right) + \dots - \mathcal{O}(1), \end{aligned} \quad (10)$$

where $\mathbf{v}_1^*, \mathbf{v}_2^*, \dots, \mathbf{v}_d^*$ denote the solutions to each subsequent max term. This sequence of solutions is the same as that returned by solving the following iterative optimization problem because maximizing mutual information with label for a linear projection of the input is the same as finding a direction that minimizes Bayes error of the linear projection (Petridis and Perantonis [41] connects mutual information to cross entropy loss and Bayes error):

1. $\mathbf{v}_1^* = \arg \min_{\|\mathbf{v}\| \leq 1} l(\langle \mathbf{v}, \mathbf{x} \rangle, y)$
2. Project data in the null space of \mathbf{v}_1^* : $(I - \mathbf{v}_1^* \mathbf{v}_1^{*\top}) \mathbf{x}$
3. Re-solve (1.) to get next \mathbf{v}_i^* and so on.

Finally, it is easy to see that solution returned by the above iterative optimization is the same as that returned by the project step of PRO².

Discussion on assumptions: Following are some remarks and intuitions behind the assumptions we make:

- **Sub-gaussianity:** We need sub-gaussianity to bound the entropy of linear projections, which is easily satisfied for inputs with bounded support. Note that the sub-gaussian parameter σ need only satisfy $\log \sigma = \mathcal{O}(1/d^2)$, where $d \ll D$ which is the input dimension of the data.
- **Bounded JS-divergence:** The main intuition behind why we need the class conditional distributions to not differ too much (bounded JS-divergence) along linear projections is that if they are very different from each other it is possible that even with sub-gaussianity assumptions there may exist linear projections that have a high mutual information over the mixture of conditionals (which is the marginal input distribution $p(\mathbf{x})$ i.e., $I(\mathbf{v}^\top \mathbf{x}; \mathbf{A}' \mathbf{x})$ is high) but not when we condition on the label (i.e., $I(\mathbf{v}^\top \mathbf{x}; \mathbf{A}' \mathbf{x} | y)$ is low). Now, since we iteratively search for linear projections, our project step is oblivious to these interactions and we may recover both of these directions (see equation 6 and Lemma 5). But only one may be present in the information theoretically optimal linear projection.

Remark on tightness of our lower bound: We show that we maximize a lower bound in equation 9. But, in the special case when the class conditionals are log-concave (e.g., multivariate Gaussian) we can also show something much tighter: $\max_{\mathbf{A} \in \mathbb{B}_d} I(\mathbf{A} \mathbf{x}; y) = \max_{\mathbf{A} \in \mathbb{B}_d} \left(\sum_{i=1}^{i=d} I(\mathbf{A}_i^\top \mathbf{x}; y) \right) - \Theta(1)$. This is because our upper bounds on the entropy terms have matching lower bounds for log-concave distributions, which can then be applied to lower bound the negative terms in the first step of equation 6.

□

We now provide proofs of the generalization bounds in Section 5 showing the bias-variance tradeoff.

Lemma 7 (generalization bound for probing projected features). *For an L -Lipshitz, B -bounded loss l , with probability $\geq 1 - \delta$, $\hat{\mathbf{w}}_d$ in equation 3 has generalization error $\lesssim \frac{\sqrt{d+B}\sqrt{\log(1/\delta)}}{\sqrt{M}}$, when $\|\mathbf{x}\|_\infty = O(1)$.*

Proof. For this proof, we invoke the following two lemmas.

Lemma 1 (generalization bound for linear functions Bartlett and Mendelson [5]). *For an L -Lipshitz B -bounded loss l , the generalization error for predictor $\hat{\mathbf{w}}_d$, contained in the class of l_2 norm bounded linear predictors \mathcal{W} is bounded with probability $\geq 1 - \delta$:*

$$l(\langle \hat{\mathbf{w}}_d, \mathbf{x} \rangle, y) - \sum_{i=1}^M l(\langle \mathbf{w}, \mathbf{\Pi}_d \mathbf{x}^{(i)} \rangle, y^{(i)}) \leq 2L\mathcal{R}_n(\mathcal{W}) + B\sqrt{\frac{\log(1/\delta)}{2M}}$$

where $\mathcal{R}_n(\mathcal{W})$ is the empirical Rademacher complexity of l_2 norm bounded linear predictors.

Lemma 2 ($\mathcal{R}_n(\mathcal{W})$ bound for linear functions [20]). *Let \mathcal{W} be a convex set inducing the set of linear functions $\mathcal{F}(\mathcal{W}) \triangleq \{\langle \mathbf{w}, \mathbf{x} \rangle : \mathcal{X} \mapsto \mathbb{R} \mid \mathbf{w} \in \mathcal{W}\}$ for some input space \mathcal{X} , bounded in norm $\|\cdot\|$ by some value $R > 0$. If there exists a mapping $h : \mathcal{W} \mapsto \mathbb{R}$ that is κ -strongly convex with respect to the dual norm $\|\cdot\|_*$ and some subset $\mathcal{W}' \subseteq \mathcal{W}$ takes bounded values of $h(\cdot)$ i.e., $\{h(\mathbf{w}) \leq K \mid \mathbf{w} \in \mathcal{W}'\}$ for some $K > 0$, then the empirical Rademacher complexity of the subset \mathcal{W}' is bounded by $\mathcal{R}_n(\mathcal{F}(\mathcal{W}')) \leq R\sqrt{\frac{2K}{\kappa n}}$.*

Let $\|\cdot\|_2^2$ be the function $h : \mathcal{W} \mapsto \mathbb{R}$ in Lemma 2; we know that $\|\cdot\|_2^2$ is 2-strongly convex in l_2 norm. Further, take the standard l_2 norm as the norm over \mathcal{X} . So, the dual norm $\|\cdot\|_*$ is also given by l_2 norm. Thus, $\kappa = 2$. We also know that \mathcal{W} is bounded in $\|\cdot\|_2$ by 1, based on our setup definition. Thus, $K = 1$.

Further, we note that $\|\mathbf{x}\|_\infty = O(1)$. We apply Cauchy-Schwartz and use the fact that $\|\mathbf{\Pi}_d\|_{\text{op}} = 1$ to bound the norm of the projected vector:

$$\|\mathbf{\Pi}_d \mathbf{x}\| \leq \|\mathbf{\Pi}_d\|_{\text{op}} \|\mathbf{x}\|_2 \leq \|\mathbf{\Pi}_d\|_{\text{op}} \sqrt{d} \|\mathbf{x}\|_\infty \lesssim \sqrt{d}. \quad (11)$$

By Lemma 2 we get the empirical Rademacher complexity $\mathcal{R}_M(\mathcal{W}) \lesssim \sqrt{d/M}$, and plugging this into Lemma 1 yields the main result in Lemma 7. \square

Theorem 8 (bias-variance tradeoff, Theorem 2). *When the conditions in Lemma 1 hold and when $\|\mathbf{x}\|_\infty = O(1)$, for B -bounded loss l , w.h.p. $1 - \delta$, the excess risk for the solution $\hat{\mathbf{w}}_d$ of PRO² that uses d features is*

$$\mathcal{L}_T(\hat{\mathbf{w}}_d) - \min_{\mathbf{w} \in \mathcal{W}} \mathcal{L}_T(\mathbf{w}) \lesssim \|(\mathbf{I}_D - \mathbf{\Pi}_d) \mathbf{w}_T^*\|_2 + \left(\frac{\sqrt{d} + B\sqrt{\log(1/\delta)}}{\sqrt{M}} \right), \quad (12)$$

where the first term of the RHS controls the bias and the second controls the variance.

Proof. The excess risk for $\hat{\mathbf{w}}_d$ is

$$\begin{aligned} & \mathcal{L}_T(\hat{\mathbf{w}}_d) - \min_{\mathbf{w} \in \mathcal{W}} \mathcal{L}_T(\mathbf{w}) \\ &= \mathcal{L}_T(\hat{\mathbf{w}}_d) - \min_{\mathbf{w} \in \text{span}\{\mathbf{\Pi}_i\}_{i=1}^d} \mathcal{L}_T(\mathbf{w}) + \min_{\mathbf{w} \in \text{span}\{\mathbf{\Pi}_i\}_{i=1}^d} \mathcal{L}_T(\mathbf{w}) - \min_{\mathbf{w} \in \mathcal{W}} \mathcal{L}_T(\mathbf{w}) \\ &= \left(\min_{\mathbf{w} \in \text{span}\{\mathbf{\Pi}_i\}_{i=1}^d} \mathcal{L}_T(\mathbf{w}) - \min_{\mathbf{w} \in \mathcal{W}} \mathcal{L}_T(\mathbf{w}) \right) + \left(\mathcal{L}_T(\hat{\mathbf{w}}_d) - \min_{\mathbf{w} \in \text{span}\{\mathbf{\Pi}_i\}_{i=1}^d} \mathcal{L}_T(\mathbf{w}) \right) \\ &\lesssim \|(\mathbf{I}_D - \mathbf{\Pi}_d) \mathbf{w}_T^*\|_2 + \left(\frac{\sqrt{d} + B\sqrt{\log(1/\delta)}}{\sqrt{M}} \right) \end{aligned} \quad (13)$$

where the first term is the bias (bounded using Lemma 1), and the second term is the generalization error or the variance (bounded using Lemma 7). \square

Corollary 9. *Under the SHOG model, $\mathbf{\Pi}_1$ recovers the linear discriminant analysis (LDA) solution, i.e., $\mathbf{\Pi}_1 = \Sigma^{-1}(\mu_2 - \mu_1) / (\|\Sigma^{-1}(\mu_2 - \mu_1)\|_2)$.*

Proof. Since the LDA solution is Bayes optimal under the HOG model, it is exactly characterized by the top eigen vector of $\Sigma^{-1}(\mu_2 - \mu_1)(\mu_2 - \mu_1)^\top$. Thus, the Bayes optimal solution on target $\mathbf{w}_T^* \propto \Sigma^{-1}(\mu_2 - \mu_1)$, and since $\mathbf{\Pi}_1$ returns the Bayes optimal linear predictor, following Theorem 6, the above corollary is proven. \square

Lemma 10 (bias under SHOG). *Let $\mathbf{\Pi}_d$ be the projection returned by PRO². The bias b_d term under our SHOG is $b_d \lesssim \|(\mathbf{I}_D - \mathbf{v}_S \mathbf{v}_S^\top) \mathbf{v}_T\|$. Here, $\mathbf{v}_S = \frac{\Sigma_S^{-1} \boldsymbol{\mu}}{\|\Sigma_S^{-1} \boldsymbol{\mu}\|_2}$ and $\mathbf{v}_T = \frac{\Sigma_T^{-1} \boldsymbol{\mu}}{\|\Sigma_T^{-1} \boldsymbol{\mu}\|_2}$. Further, when $\|\Sigma_S\|_{\text{op}}$ is bounded, and $\mathbf{\Pi}_d$ is a random rank d projection matrix, $b_d = O\left(\sqrt{1 - \frac{d}{D}} \cdot \text{KL}(p_S \| p_T)\right)$.*

Proof. From Corollary 9, we know that $\mathbf{\Pi}_1$ is exactly the rank-1 projection matrix given by the direction $\Sigma_S^{-1}(\mu_2 - \mu_1)/(\|\Sigma_S^{-1}(\mu_2 - \mu_1)\|_2)$. Therefore

$$b_d \leq \|(\mathbf{I}_D - \mathbf{\Pi}_d)\mathbf{w}_T^*\|_2 \leq \|(\mathbf{I}_D - \mathbf{\Pi}_1)\mathbf{w}_T^*\|_2 = \|(\mathbf{I}_D - \mathbf{v}_S\mathbf{v}_S^\top)\mathbf{v}_T\|. \quad (14)$$

This gives us the first result for $\mathbf{v}_S, \mathbf{v}_T$.

For the second result, we note that the KL divergence between multivariate Gaussian distributions is convex.

$$\begin{aligned} \text{KL}(p_S||p_T) &= \text{KL}(p(y)p_S(\mathbf{x} | y)||p(y)p_T(\mathbf{x} | y)) \\ &\leq \text{KL}(p_S(\mathbf{x} | y)||p_T(\mathbf{x} | y)) \\ &= 0.5 \cdot \text{KL}(\mathcal{N}(\mu_1, \Sigma_S)||\mathcal{N}(\mu_1, \Sigma_T)) + 0.5 \cdot \text{KL}(\mathcal{N}(\mu_2, \Sigma_S)||\mathcal{N}(\mu_2, \Sigma_T)) \\ &= \frac{1}{2}\text{tr}(\Sigma_T^{-1}\Sigma_S) - \sum_{i=1}^D \log \lambda_i^S + \sum_{i=1}^D \log \lambda_i^T - D. \end{aligned} \quad (15)$$

Refer to Wainwright [56] for the final step, where λ_i^S and λ_i^T are the eigenvalues of source and target covariance matrices, respectively. The final term in the above derivation is $\mathcal{O}(\text{tr}(\Sigma_T^{-1}))$ when $\|\Sigma_S\|_{\text{op}} = \mathcal{O}(1)$. From Lemma 1 we know that under random projections onto d dimensions,

$$b_d \leq L \cdot \sqrt{1 - (d/D)} \|\mathbf{w}_T^*\| \lesssim \sqrt{1 - (d/D)} \|\Sigma_T^{-1}(\mu_2 - \mu_1)\| \lesssim \text{tr}(\Sigma_T^{-1}) \quad (16)$$

where we use Corollary 9. Thus from (16) and (15), we get our desired bound:

$$b_d \lesssim \left(\sqrt{1 - \frac{d}{D}} \cdot \text{KL}(p_S||p_T) \right).$$

□

Corollary 11 (tradeoff under SHOG, Corollary 3). *Under our SHOG model of shift, and conditions for a random projection $\mathbf{\Pi}_d$ in Lemma 10, the target error $\mathcal{L}_T(\hat{\mathbf{w}}_d) \lesssim \mathcal{O}\left(\sqrt{1 - \frac{d}{D}} \cdot \text{KL}(p_S||p_T)\right) + \sqrt{\frac{d}{M}}$, when $\|\Sigma_T\|_{\text{op}} = \mathcal{O}(1)$.*

Proof. Direct application of the variance result in Lemma 7 and bias result in Lemma 10, using the same technique used to prove Theorem 2. □

B Experimental Details

B.1 PyTorch pseudocode for the projection step

Below, we provide PyTorch pseudocode for the projection step of PRO² for binary classification datasets.

```
def learn_feature_space_basis(x, y, num_features):
    projection = torch.nn.Linear(x.shape[1], num_features)
    opt = torch.optim.AdamW(projection.parameters(), lr=0.01,
                             weight_decay=0.01)

    max_steps = 100
    for i in range(max_steps):
        logits = projection(x)
        loss = F.binary_cross_entropy_with_logits(logits, y, reduction
                                                    = "none").mean()

        opt.zero_grad()
        loss.backward()
        opt.step()
        # Enforce orthogonality; we're performing projected gradient
        # descent
        Q, R = torch.linalg.qr(projection.weight.detach().T)
        projection.weight.data = (Q * torch.diag(R)).T
    feature_space = projection.weight.detach().T
    return feature_space
```


B.2 Additional dataset details

- **4-Way Collages** [51]. This binary classification dataset consists of 4-way collages of four images per datapoint, one from each of (1) CIFAR, (2) MNIST, (3) Fashion-MNIST, and (4) SVHN. All four image features are completely correlated in the source data, and we consider four target distributions, where only one of the image features are predictive of the label in each target distribution.
- **Waterbirds** [44]. This dataset tasks the model with classifying images of birds as either a waterbird or landbird. The label is spuriously correlated with the background of the image, which is either water or land. There are 4,795 training samples, of which 95% of the data follows the spurious correlation. We use the original training set as the source data and evaluate on 3 different target distributions constructed from the original test dataset: (1) Minority, which contains the test data points that do not follow the spurious correlation, (2) Spurious, containing the points that do, and (3) Balanced, which contains an equal number of points from each of the 4 (bird, background) groups.
- **CelebA** [32]. Similar to Waterbirds, we use the original training set as source data and evaluate on (1) Minority, (2) Spurious, and (3) Balanced target distributions. In our main experiments in Sec. 6, we use target distributions corresponding to the spurious correlation typically used for evaluation (spurious attribute–gender with label–hair color). Below, in Appendix C include additional results on 4 other variants following the settings used in [27]: (1) CelebA-1 uses slightly open mouth as the label and wearing lipstick as the spurious attribute, (2) CelebA-2 uses attractive as the label and smiling as the spurious attribute, (3) CelebA-3 uses wavy hair as the label and high cheekbones as the spurious attribute, and finally (4) CelebA-4 uses heavy makeup as the label and big lips as the spurious attribute.
- **Camelyon17** [4]. This dataset is part of the WILDS benchmark [22] and contains medical images where variations in data collection from different hospitals induce naturally occurring distribution shifts. We evaluate on 2 target distributions: (1) ID-Test: a held out test set of images from the source distribution, and (2) OOD-Test: the actual test distribution with a distribution shift due to evaluating data from a different hospital.
- **Living17** [45]. The task is to classify images into one of 17 animal categories. This dataset presents a subpopulation shift, in that while the ID and OOD distributions have the same overall classes, they contain different subpopulations. We test on the given test set.
- **FMoW** [22]. This dataset contains satellite images from 5 geographic regions, and the task is to classify the image as one of 62 building or land use types. For the target distribution, we use the subset of the OOD test data belonging to the Africa region.

Pre-trained models and additional training details. We extract penultimate embeddings of all source and target datapoints from a pre-trained backbone. We preprocess all datapoints according to the augmentation used during pre-training, and obtain feature embeddings with eval-mode batch normalization. We cache all embeddings for a (backbone, dataset) pair to a single file and train our linear models from the cached file. We use CLIP-ViT-L/16 [11] in our main experiments, and additionally experiment with ResNet18 [17], ResNet50, ResNet50-SWaV [6], CLIP-ViT-B/16 models in Appendix C.3. All pretrained models are publicly available online. We train all models using the AdamW optimizer [33] with weight decay 0.01. For all experiments, we perform early stopping with accuracy on held-out target data and report mean and standard deviation across 10 runs.

C Additional Experimental Results

C.1 Additional visualizations for synthetic Gaussian experiment

In Fig. 6, we approximate the bias and variance in the synthetic HOG experiment studied in Fig. 3. On the left, for each test distribution (ID, Near OOD, and Far OOD), we plot the relationship between approximate bias (using error at the largest target dataset size) and nullspace norm and find that they have a roughly linear relationship. Thus, this plot empirically supports the connection supported in the theory between bias and the number of features used, as the nullspace norm decreases as the dimension of the feature-space basis increases.

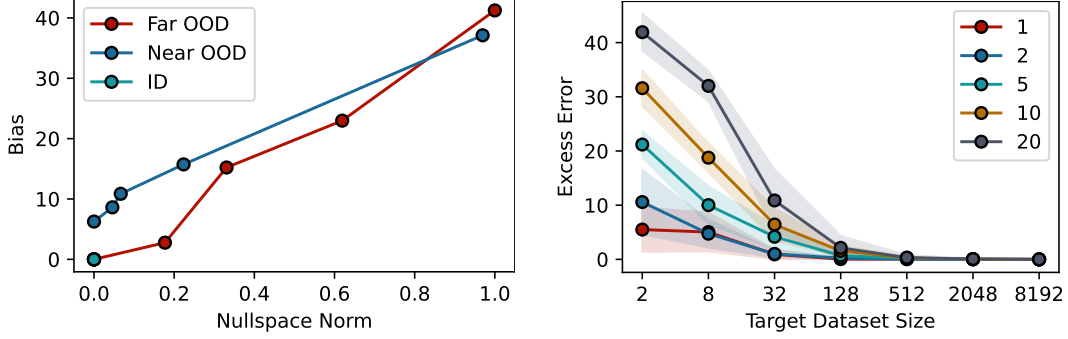


Figure 6: Visualization of bias and variance in the synthetic homoscedastic Gaussian experiment Fig. 3. (Left) We approximate bias by the error at the largest target dataset size, and compare to the nullspace norm. The two quantities have a roughly linear relationship. (Right) We approximate variance by the difference between the error at each dataset size and the error at the largest. We report the average across the three test distributions. Note on the left plot, ID is easily learned and so the corresponding line is therefore clustered near $(0, 0)$, as the nullspace norm and bias are both near 0.

C.2 Empirical analysis of projected feature space

We begin by observing the empirical properties of the projected feature space learned during the first projection phase of PRO². The Waterbirds dataset consists of “spurious” groups where the background type (land or water) correlates with the bird type (land or water), on which using a shortcut feature that relies on background type will perform optimally, as well as “minority” groups in which the correlation does not hold and requires a robust feature that focuses on the bird itself. On this dataset, we first extract oracle shortcut and robust features by minimizing loss on spurious and minority groups on target data, respectively. These two directions serve as proxies for the optimal classifier on two different target distributions. In addition to PRO², we also evaluate a random feature extraction method, which simply samples a random orthonormal basis for the original \mathbb{R}^D embedding space. We plot the nullspace norm of these two features in the subspace spanned by the first k directions, for $1 \leq k \leq D = 1024$ in ?? . As expected, we see that the earlier features learned by PRO² are more similar to the shortcut feature than the robust feature. Because the orthogonality constraint forces the features to be different from each other, the nullspace norm reduces to zero at the highest value $k = 1024$. This experiment shows that the basis learned by PRO² contains both the robust and shortcut features for this dataset, and that the robust and shortcut features emerge even for very low-rank bases (i.e., for small values of d). In contrast, a random orthogonal basis only captures these two predictive features when the rank is larger. This indicates that our orthogonal projection approach quickly picks up on the most important directions in feature space, which in this case correspond to the shortcut feature representing the background and the robust feature representing the type of bird, as discussed in prior work [44].

C.3 Using various pretrained backbones

Finally, as PRO² relies on using a pre-trained backbone model that is not fine-tuned to initially extract features, we study how different backbones affect performance. In Fig. 7, we plot the accuracy of PRO² using 5 pre-trained backbone models that achieve a range of Image-Net accuracies. We find that PRO² improves significantly with better pre-trained backbones. These experiments demonstrate the promise of the PRO² framework. The quality of pre-trained feature extractors will continue to improve with future datasets and architectures, and PRO² leverages such pre-trained backbone models for distribution-shift adaptation in a computationally efficient manner.

C.4 Ablation on the importance of enforcing orthogonality

For the purposes of our empirical analysis, we additionally consider a simpler variant that optimizes the projection matrix Π with No Constraint on orthogonality:

$$\Pi_i = \arg \min \mathbb{E}_{(x,y) \sim \mathcal{D}_S} \mathcal{L}(\Pi_i(f(x)), y). \quad (\text{PRO}^2\text{-NC})$$

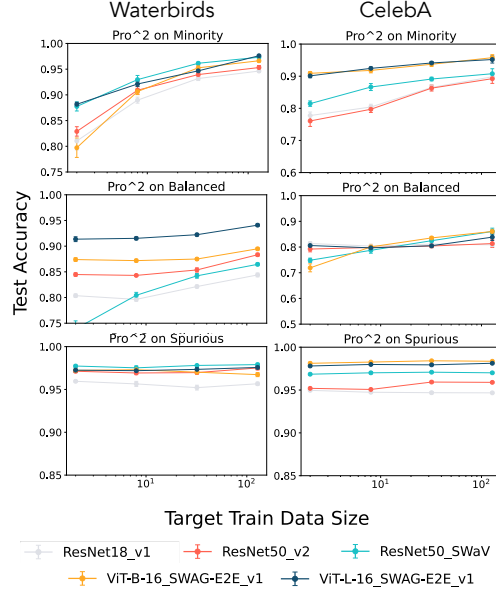


Figure 7: **Different backbones.** We show the accuracy of PRO^2 , where we use various pretrained backbones, which are not fine-tuned. PRO^2 is able to leverage improvements in the backbone with minimal computational overhead.

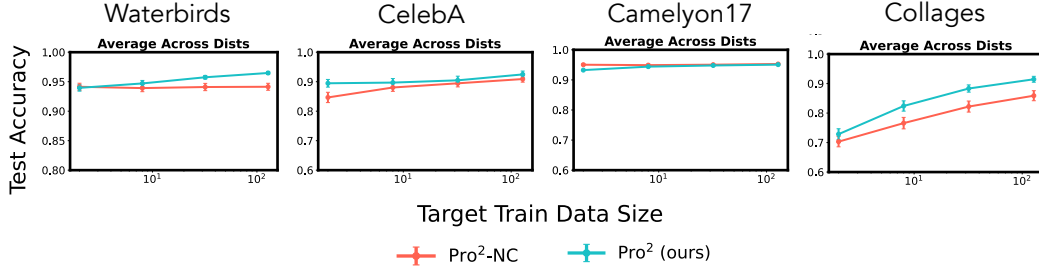


Figure 8: **Importance of orthogonality.** We show the adaptation accuracy of PRO^2 compared to $\text{PRO}^2\text{-NC}$, a variant without orthogonality enforced, averaged across the varying target distributions for each dataset.

We compare PRO^2 to $\text{PRO}^2\text{-NC}$ in Fig. 8. While $\text{PRO}^2\text{-NC}$ is sufficient in some scenarios with milder distribution shift, where the shortcut feature continues to be informative, it fails to learn a diverse set of predictive features and often only learns shortcut features, often failing on more severe distribution shifts.

C.5 Evaluation on additional CelebA variants

Finally, in Fig. 9 we supplement our main results in Fig. 4 with additional results from 4 additional variants of CelebA. The takeaways from these results line up with those from Fig. 4. In the few-shot adaptation problem setting, PRO^2 is consistently the most effective, compared to Random Projection, DFR [21], which uses standard linear probing, and [51].

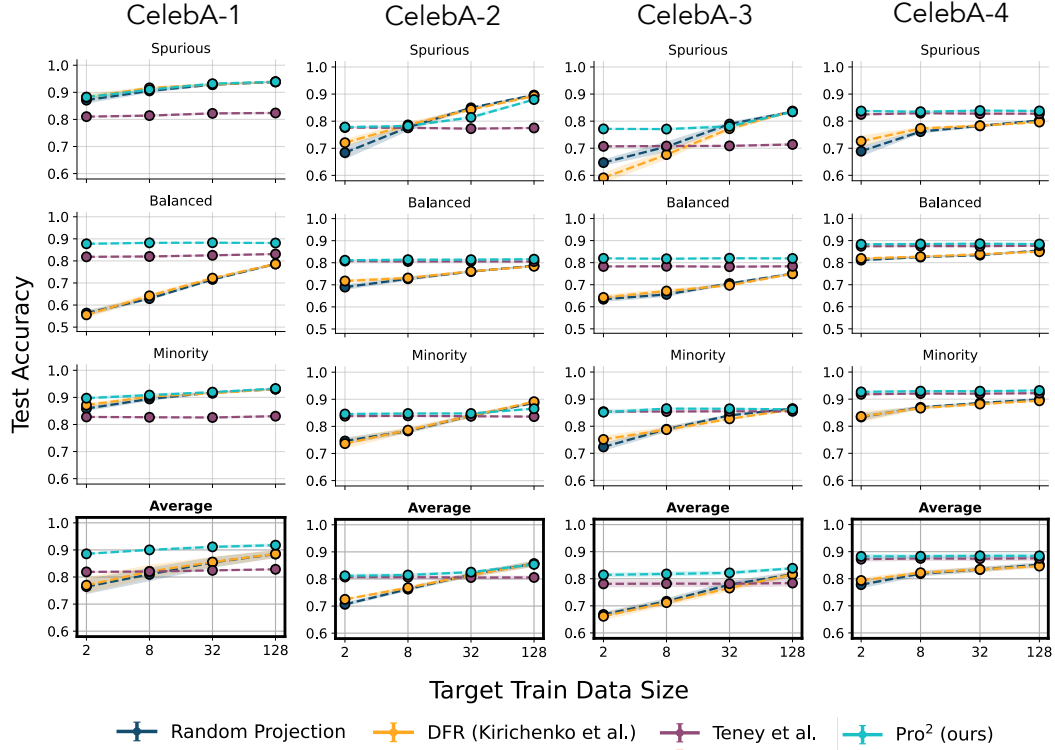


Figure 9: **Main results on additional CelebA variants.** We compare 4 different methods for learning features to adapt to a target distribution: (1) Random Projection, (2) DFR Kirichenko et al. [21], i.e. standard linear probing, (3) [51], and (4) PRO². We report target accuracies after probing with different target dataset sizes; we report mean and standard deviation across 10 runs. Similar to the trends seen in Fig. 4, PRO² achieves high accuracy in the low-data regime, substantially outperforming both random orthogonal projection and no projection in most target distributions on all four datasets.